



# Kinetics of zircon formation in yttria partially stabilized zirconia as a result of oxidation of embedded molybdenum disilicide

Franck Nozahic, Alexandra Lucia Carabat, Weichen Mao, Daniel Monceau, Claude Estournès, Cornelis Kwakernaak, Sybrand van Der Zwaag, Willem G. Sloof

## ► To cite this version:

Franck Nozahic, Alexandra Lucia Carabat, Weichen Mao, Daniel Monceau, Claude Estournès, et al.. Kinetics of zircon formation in yttria partially stabilized zirconia as a result of oxidation of embedded molybdenum disilicide. *Acta Materialia*, 2019, 174, pp.206-216. 10.1016/j.actamat.2019.05.046 . hal-02160992

**HAL Id: hal-02160992**

**<https://hal.science/hal-02160992>**

Submitted on 20 Jun 2019

**HAL** is a multi-disciplinary open access archive for the deposit and dissemination of scientific research documents, whether they are published or not. The documents may come from teaching and research institutions in France or abroad, or from public or private research centers.

L'archive ouverte pluridisciplinaire **HAL**, est destinée au dépôt et à la diffusion de documents scientifiques de niveau recherche, publiés ou non, émanant des établissements d'enseignement et de recherche français ou étrangers, des laboratoires publics ou privés.






## Open Archive Toulouse Archive Ouverte (OATAO)

OATAO is an open access repository that collects the work of Toulouse researchers and makes it freely available over the web where possible

This is an author's version published in: <http://oatao.univ-toulouse.fr/24028>

**Official URL:** <https://doi.org/10.1016/j.actamat.2019.05.046>

### To cite this version:

Nozahic, Franck  and Carabat, Alexandra Lucia and Mao, Weichen and Monceau, Daniel  and Estournès, Claude  and Kwakernaak, Cornelis and van der Zwaag, Sybrand and Sloof, Willem G. *Kinetics of zircon formation in yttria partially stabilized zirconia as a result of oxidation of embedded molybdenum disilicide*. (2019) Acta Materialia, 174. 206-216. ISSN 1359-6454

Any correspondence concerning this service should be sent  
to the repository administrator: [tech-oatao@listes-diff.inp-toulouse.fr](mailto:tech-oatao@listes-diff.inp-toulouse.fr)

# Kinetics of zircon formation in yttria partially stabilized zirconia as a result of oxidation of embedded molybdenum disilicide

F. Nozahic<sup>a, b</sup>, A.L. Carabat<sup>c</sup>, W. Mao<sup>c</sup>, D. Monceau<sup>a</sup>, C. Estournes<sup>b</sup>, C. Kwakernaak<sup>c</sup>, S. van der Zwaag<sup>d</sup>, W.G. Sloof<sup>c, \*</sup>

<sup>a</sup> CIRIMAT, Université de Toulouse, CNRS, INPT, UPS, ENSIACET, 4 allée Emile Monso, 31030 Toulouse, France

<sup>b</sup> CIRIMAT, Université de Toulouse, CNRS, INPT, UPS, 118 Route de Narbonne, F-31062 Toulouse, France

<sup>c</sup> Department of Materials Science and Engineering, Delft University of Technology, Mekelweg 2, 2628 CD, Delft, the Netherlands

<sup>d</sup> Faculty of Aerospace Engineering, Delft University of Technology, Kluyverweg 1, 2629 HS, Delft, the Netherlands

## ARTICLE INFO

### Keywords:

Yttria partially stabilized zirconia  
Molybdenum disilicide  
Interdiffusion  
Zircon formation kinetics  
Self-healing

## ABSTRACT

Recently MoSi<sub>2</sub> sacrificial particles embedded in yttria partially stabilized zirconia (YPSZ) have been proposed as attractive healing agents to realize significant extension of the lifetime of the thermally loaded structures. Upon local fracture of the YPSZ, the embedded healing particles in the path and in the vicinity of the crack react with the oxygen atoms transported via the crack and first fill the crack with a viscous glassy silica phase (SiO<sub>2</sub>). The subsequent reaction between this freshly formed SiO<sub>2</sub> and the existing tetragonal ZrO<sub>2</sub> of the YPSZ leads to the formation of rigid crystalline zircon (ZrSiO<sub>4</sub>), which is key in the crack-healing mechanism of YPSZ based materials. The isothermal kinetics of the self-healing reaction and the mechanism of zircon formation from the decomposing MoSi<sub>2</sub> and the surrounding YPSZ were assessed via X-ray diffraction (XRD). The obtained results revealed that at 1100 °C the reaction between amorphous SiO<sub>2</sub> and YPSZ is completed after about 10 h. For a more accurate determination of the kinetics of the self-healing reaction, bilayer samples of YPSZ – MoSi<sub>2</sub> (with and without boron addition) were annealed in air over a temperature range of 1100–1300 °C. This led to the formation of a MoSi<sub>2</sub>/amorphous (boro)silica/zircon/YPSZ multi-layer, which was investigated with scanning electron microscopy (SEM) and electron probe X-ray microanalysis (EPMA). Kinetic modeling of the growth of zircon and silica or borosilicate layers showed that zircon growth was dominated by the diffusion of Si<sup>4+</sup> in zircon whereas the growth of the silica or borosilicate layer was controlled by oxygen diffusion. Moreover, a significant increase in the rate of ZrSiO<sub>4</sub> formation was observed due to the presence of B in the MoSi<sub>2</sub> particles.

## 1. Introduction

A concept of crack-healing in yttria partially stabilized zirconia (YPSZ, i.e. ZrO<sub>2</sub> containing 4–5 mol % Y<sub>2</sub>O<sub>3</sub>) has been proposed, which involves molybdenum disilicide (MoSi<sub>2</sub>) sacrificial particles embedded in a YPSZ ceramic matrix that respond to crack formation [1]. At high-temperatures in an oxidizing gas environment, the MoSi<sub>2</sub> particles in the crack path forms a glassy silica (SiO<sub>2</sub>) flowing into the crack-gap and reconnecting the fracture surfaces. Subsequently, the silica formed reacts with the matrix, resulting in the formation of crystalline zircon (ZrSiO<sub>4</sub>) phase which, unlike the

viscous silica, has a mechanical load bearing ability at high temperatures [2]. As the final healing product, ZrSiO<sub>4</sub>, is key in re-establishing the mechanical integrity of YPSZ, the mechanism and kinetics that governs its formation is highly relevant for the effective kinetics of strength restoration of damaged YPSZ and is therefore studied here.

The kinetics of silica formation as a result of MoSi<sub>2</sub> oxidation at high-temperature is well documented, e.g. Ref. [3]. However, comprehensive knowledge on the kinetics and mechanism of the subsequent zircon formation due to SiO<sub>2</sub> reacting with ZrO<sub>2</sub> is lacking. So far, only the formation of zircon from a mixture of zirconia and silica in the form of quartz, cristobalite, tridymite and amorphous phase has been studied [4]. The reaction between zirconia and silica requires temperatures above 1300 °C and the allotropic modification of silica has little or no effect on the final

\* Corresponding author.

E-mail address: [w.g.sloof@tudelft.nl](mailto:w.g.sloof@tudelft.nl) (W.G. Sloof).

degree of zircon formation [4], whereas  $\text{ZrSiO}_4$  could be formed from an equimolar mixture of amorphous  $\text{SiO}_2$  and  $\text{ZrO}_2$  at 1200 °C [4,5]. Also, it has been observed that the formation of zircon from amorphous  $\text{SiO}_2$  and tetragonal zirconia (t- $\text{ZrO}_2$ ) predominates over the allotropic transformation of amorphous silica to cristobalite [4]. In addition, only a few studies dealt with the actual reaction mechanism of zircon formation [4–6]. The available data claims that zircon precipitates at the interface between  $\text{ZrO}_2$  and  $\text{ZrSiO}_4$  once the solubility limit of Si in zirconia is reached. However, this is not supported yet by experimental evidence like element concentration profiles along the  $\text{ZrSiO}_4$  layer. A complete description of the reaction kinetics between  $\text{ZrO}_2$  and  $\text{SiO}_2$ , including determination of the activation energy of zircon formation is needed, since the existing data accounts only for the formation of  $\text{ZrSiO}_4$  starting from  $\text{SiO}_2$  (including its allotropes) and only unstabilized zirconia.

The formation of amorphous silica covering the surface upon oxidation of  $\text{MoSi}_2$  (and  $\text{Mo}_5\text{Si}_3$ ) is promoted by addition of boron as  $\text{MoB}$  [7–12], thereby mitigating the formation of volatile  $\text{MoO}_3$  [13]. At relatively low oxidation temperatures, in the range of 600–800 °C, the formation of this gaseous  $\text{MoO}_3$  is considered to be responsible for the rapid oxidation and associate disintegration of molybdenum silicides, also known as ‘pest oxidation’ [14–16].

Recent studies have indicated that the presence of boron in the  $\text{MoSi}_2$  particles can increase the fluidity of the amorphous  $\text{SiO}_2$  formed [2,17,18], a feature which is likely to enhance the subsequent reaction kinetics of  $\text{SiO}_2$  with the  $\text{ZrO}_2$  being the main constituent of YPSZ. Therefore, the work presented here focuses on the zircon formation from YPSZ and boron-free and boron containing  $\text{MoSi}_2$  at high temperatures in an oxidizing gas environment. First, the zircon formation is studied of a mixture of both YPSZ and  $\text{MoSi}_2$  (with and without B) powders. Next, the kinetics of zircon formation is determined quantitatively for YPSZ- $\text{MoSi}_2$  (with and without B) bilayer samples.

This work is relevant for the development of a self-healing thermal barrier coating (TBC) system [1,19–22]; see Fig. S1 in Supplementary Information. To date ceramic thermal barrier coatings (TBCs) are applied on the surface of hot-section metallic components in advanced gas turbine engines to protect them from corrosion and oxidation at elevated temperatures and to lower the temperature of the metallic substrate [23–27]. Depending on the thickness and the porosity of the TBCs, the temperature of the metallic substrates is reduced by 100–300 °C [23,25,27–29], allowing higher operating temperatures in the combustion chamber itself [30] and, hence, increasing the turbine engine efficiency [31]. YPSZ is the state of art of the current TBCs owing to its excellent chemical and thermo-mechanical properties, such as low thermal conductivity at elevated temperatures ( $2.3 \text{ W m}^{-1} \text{ K}^{-1}$  at 1000 °C), low density ( $6.4 \text{ g cm}^{-3}$ ), high melting point (2700 °C), appreciable toughness ( $7.7 \text{ MPa m}^{0.5}$ ) and good corrosion resistance [23,25,26]. However, unavoidably residual stresses [23,32–34] develop due to the difference in the coefficient of thermal expansion (CTE) between the YPSZ ceramic top coat (CTE is  $10\text{--}11 \cdot 10^{-6} \text{ °C}^{-1}$ ) [35] and the underlying metal substrate, commonly a Ni-based superalloy (CTE is  $14 \cdot 10^{-6} \text{ °C}^{-1}$ ) [28]. Upon thermal cycling these stresses initiate micro-cracks within the brittle ceramic coating, which propagate and coalesce causing spallation of the TBC [23,36–42]. As a result, the metallic components are locally directly exposed to the high temperature environment which can lead to local melting or local thermal damage [23,40].

The current material of choice for TBCs does not exhibit autonomous crack-healing capabilities, therefore self-repair mechanisms [43] that can be executed at high temperature and directly upon damaged sections may represent a viable solution to prolong the lifetime of the ceramic top coat.

## 2. Experimental procedure

### 2.1. Materials and sample preparation

To study the zircon formation mechanism and kinetics in equimolar mixtures of YPSZ (with 5 mol%  $\text{Y}_2\text{O}_3$ ) powder with  $\text{MoSi}_2$  (without and with 9 at.% B) at high temperatures in air, 70% dense pellets were prepared. Commercial YPSZ with 5 mol%  $\text{Y}_2\text{O}_3$  was used (Sulzer NS 204, average particle size 45  $\mu\text{m}$ ). The  $\text{MoSi}_2$  powders without and with B were supplied by ChemPur GmbH, Germany, with 99.5 and 99% purity and average particle size of 5 and 18  $\mu\text{m}$ , respectively. Henceforth, the  $\text{MoSi}_2$  particles doped with B are denoted as  $\text{MoSi}_2(\text{B})$ , while the B-free particles are denoted as  $\text{MoSi}_2$ .

For the interdiffusion experiments, bilayer samples of YPSZ –  $\text{MoSi}_2$  and YPSZ –  $\text{MoSi}_2(\text{B})$  were prepared using spark plasma sintering (SPS); see Ref. [44] for details of the equipment. First, B-free and B-containing  $\text{MoSi}_2$  samples were produced with a relative density better than 99%. Specimens of  $5 \times 5 \times 0.5 \text{ mm}$  with parallelepiped-like shape were cut from the sintered materials. All surfaces of the  $\text{MoSi}_2$  specimens were finely polished using 1  $\mu\text{m}$  diamond grains in the final step. These pieces were placed in a 20 mm inner diameter graphite die and, on both sides, covered with YPSZ powder. In this case, the YPSZ powder used was Amperit 827.774 (with 4–5 mol%  $\text{Y}_2\text{O}_3$ ) that was downsized to an average particle size of 7  $\mu\text{m}$  with a planetary ball mill. The sintering was performed at 1500 °C (heating rate of 100 °C/min) and a soaking time of 30 min, applying a uni-axial pressure of 120 MPa applied from the beginning of sintering cycle. DC pulses were applied following the standard 12/2 (on/off 3.3 ms) sequence. After sintering, the  $\text{MoSi}_2$  sample is embedded in YPSZ at the center and intimate contact between the materials is established; see Fig. 2a in Supplementary Information. Inside the SPS equipment and near the sample the oxygen partial pressure is governed by the equilibrium between the C (graphite die) and  $\text{O}_2$ , CO and  $\text{CO}_2$  gases, which results in an oxygen partial pressure of  $5 \cdot 10^{-17} \text{ Pa}$ . The oxygen partial pressure required to form  $\text{SiO}_2$  at 1500 °C is about  $10^{-18} \text{ Pa}$ . These conditions in combination with the prolonged dwell time at 1500 °C may result in the formation of a thin silica or borosilicate layer during the manufacturing.

### 2.2. Isothermal annealing of powder mixtures and diffusion couples

The isothermal annealing experiments of the green tablets were performed in an open horizontal alumina tube furnace at 1100 and 1200 °C for 0.5 up to 15 h. After annealing, the samples were quickly removed from the hot-zone and cooled down rapidly in ambient air. Similarly, the bilayer samples were annealed in laboratory air at temperatures ranging from 1100 to 1300 °C and exposure times ranging from 48 up to 240 h.

### 2.3. Methods of investigation

The crystalline phases of the composite pellets were identified after each annealing period with X-ray diffractometry (XRD) using monochromated  $\text{Cu-K}\alpha_1$  radiation (154.060 p.m. wavelength). The diffractograms were recorded in the  $2\theta$  range of 15 to 90°.

XRD analysis was also employed to quantify the near surface evolution of  $\text{ZrO}_2$  consumption and  $\text{ZrSiO}_4$  formation with annealing time and temperature. To this end, the intensity of  $\text{ZrO}_2$  peaks corresponding to the monoclinic and tetragonal phases (112) and (020) were recorded after each annealing period within the  $2\theta$  range of 48 to 52°. Similarly, the intensity of  $\text{ZrSiO}_4$ -(200) peak intensity was observed in the  $2\theta$  range of 26 to 31° to



determine the  $\text{ZrSiO}_4$  formation. In both cases, the net integrated peak intensity was considered as a measure of the amount of  $\text{ZrO}_2$  and  $\text{ZrSiO}_4$  in the samples. The ratio between the net integrated intensity before and after each annealing time was determined to obtain the fraction of unreacted  $\text{ZrO}_2$  and formed  $\text{ZrSiO}_4$ , assuming that no texture had developed in the sample during the annealing treatment.

The microstructures of the annealed composite tablets and bilayers were investigated with scanning electron microscopy (SEM). To this end, cross-sections were prepared by cutting the pellets and the bilayer samples in half; see Fig. S2a in Supplementary Information.

The thicknesses of silica and zircon layers were measured using an image analysis program (PhotoImpact 8). First, the recorded backscattered images were converted into binary images to separate the two layers. Thereafter, the total number of pixels over the length of the layers was counted to obtain the thickness values of silica and zircon layer after each exposure temperature and time. An example of a processed backscattered image along with the calculated thicknesses of borosilicate and  $\text{ZrSiO}_4$  layer is displayed in Figs. S2b and S2c in Supplementary Information.

The local compositions and composition profiles of the bilayer samples were obtained with electron probe X-ray microanalysis (EPMA) using wavelength dispersive spectrometry (WDS). The composition at each analysis location of the sample was determined using the X-ray intensities of the constituent elements after background correction relative to the corresponding intensities of the reference materials. The measured intensity ratios were processed with a matrix correction program CITZAF to yield the actual composition [45].

### 3. Results

#### 3.1. Oxidation phenomena

Exposure of the compacted equimolar mixtures of YPSZ powder with  $\text{MoSi}_2$  or  $\text{MoSi}_2(\text{B})$  at high temperatures in air resulted in the formation of silica ( $\text{SiO}_2$ ) or borosilicate ( $\text{SiO}_2\text{--B}_2\text{O}_3$ ) due to oxidation of the  $\text{MoSi}_2$  particles; see Fig. 1a and b. These oxides completely fill the space between YPSZ and the  $\text{MoSi}_2$ . The oxidation of Si originating from the  $\text{MoSi}_2$  and  $\text{MoSi}_2(\text{B})$  particles resulted in the formation of  $\text{Mo}_5\text{Si}_3$ ; see also Refs [46–49]. The formation of borosilicate causes a partial breakup of the Si–O bonds in the silica network, which changes its properties, such as melting point, wettability and viscosity according to Refs. [17,18,50–56].

Subsequently,  $\text{SiO}_2$  reacts with t- $\text{ZrO}_2$  of the YPSZ forming  $\text{ZrSiO}_4$  at the outer side or rim of the YPSZ particles according to:



XRD analyzes show that in addition to  $\text{ZrSiO}_4$ , also  $\text{Mo}_5\text{Si}_3$  and crystalline  $\text{SiO}_2$  (cristobalite) were formed; see Fig. 2a. Amorphous silica, which forms during  $\text{MoSi}_2$  oxidation, tends to transform into cristobalite prior or during reaction with  $\text{ZrO}_2$  [3,46,49]. Also, some  $\text{Y}_2\text{Si}_2\text{O}_7$  is observed, which suggests a reaction between the remaining amorphous  $\text{SiO}_2$  and  $\text{Y}_2\text{O}_3$  [57].

However, when boron is present in  $\text{MoSi}_2$ , the rate of silica formation as borosilicate is enhanced and the formation of  $\text{ZrSiO}_4$  is promoted. After annealing an equimolar mixture of YPSZ and  $\text{MoSi}_2$  with 9 at.% B at  $1200^\circ\text{C}$  for 15 h, only a few unreacted  $\text{MoSi}_2$  particles with  $\text{Mo}_5\text{Si}_3$  could be detected; see Fig. 2b. The presence of boron led to the formation of amorphous borosilicate according to XRD analysis and EPMA; see also e.g. Refs. [9,16,52,54,55,58]. After oxidation at  $1100^\circ\text{C}$  some crystalline  $\text{SiO}_2$  cristobalite was observed, but after oxidation at  $1200^\circ\text{C}$

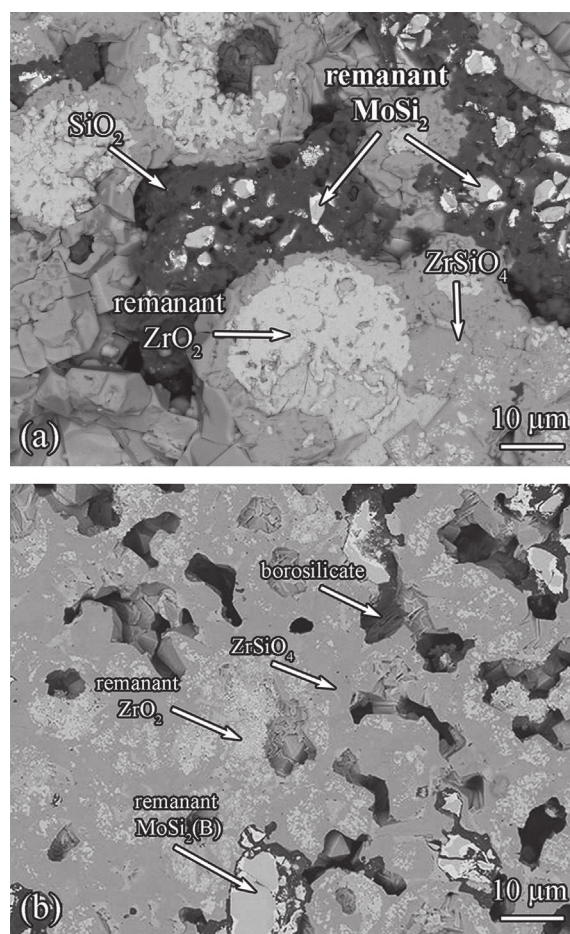


**Fig. 1.** Cross-section image of (a) YPSZ –  $\text{MoSi}_2$  and (b) YPSZ –  $\text{MoSi}_2(\text{B})$  tablets after annealing at  $1200^\circ\text{C}$  in laboratory air for 15 h. Corroborated with X-ray microanalysis, five main phases were identified: (1) Bright pebble like particles are remnant  $\text{MoSi}_2$  and  $\text{MoSi}_2(\text{B})$  particles, respectively. (2) The bright phase at the edge of  $\text{MoSi}_2$  and  $\text{MoSi}_2(\text{B})$  belongs to  $\text{Mo}_5\text{Si}_3$ . (3) The darker region represents  $\text{SiO}_2$  and borosilicate, respectively. (4) The grey region between  $\text{SiO}_2$  or borosilicate and  $\text{ZrO}_2$  is the reaction product of these two components, namely  $\text{ZrSiO}_4$ . (5) The whitish area is remnant  $\text{ZrO}_2$ .

only amorphous borosilicate was formed. This suggests that the presence of B precludes the crystallization of the amorphous  $\text{SiO}_2$  to cristobalite, cf [56]. Moreover, in contrast to the oxidation reaction between the YPSZ and  $\text{MoSi}_2$  particles, no  $\text{Y}_2\text{Si}_2\text{O}_7$  was observed; see Fig. 2b. However, the acidic nature of the  $\text{B}_2\text{O}_3$  and the high annealing temperature,  $\text{B}_2\text{O}_3$  can promote the removal of yttrium ions from YPSZ [59]. This may lead to the formation of glassy  $\text{YBO}_3$  and monoclinic zirconia (m- $\text{ZrO}_2$ ), but is not observed here.

XRD analyzes of the YPSZ powder, used in the compacted powder mixtures (see Section 2.1), is composed mainly of t- $\text{ZrO}_2$  with small amount of m- $\text{ZrO}_2$ , which not changed after exposure for at  $1200^\circ\text{C}$  for 15 h in air. In the XRD pattern of the YPSZ powder used for preparing the bilayer samples with SPS (see Section 2.1) only t- $\text{ZrO}_2$  and no m- $\text{ZrO}_2$  nor cubic zirconia (c- $\text{ZrO}_2$ ) was observed. Also, after SPS the compact consisted only of t- $\text{ZrO}_2$ . After long exposure at high temperatures a minute amount of m- $\text{ZrO}_2$  was traceable. According to the zirconia-yttria phase diagram [60], in the YPSZ with 4–5 mol%  $\text{Y}_2\text{O}_3$  powder only m- $\text{ZrO}_2$  and c- $\text{ZrO}_2$  are stable at room temperature. At high temperatures (above about  $550^\circ\text{C}$ ) the tetragonal phase is stable. However, since the diffusion of Y ions in zirconia is slow and the driving

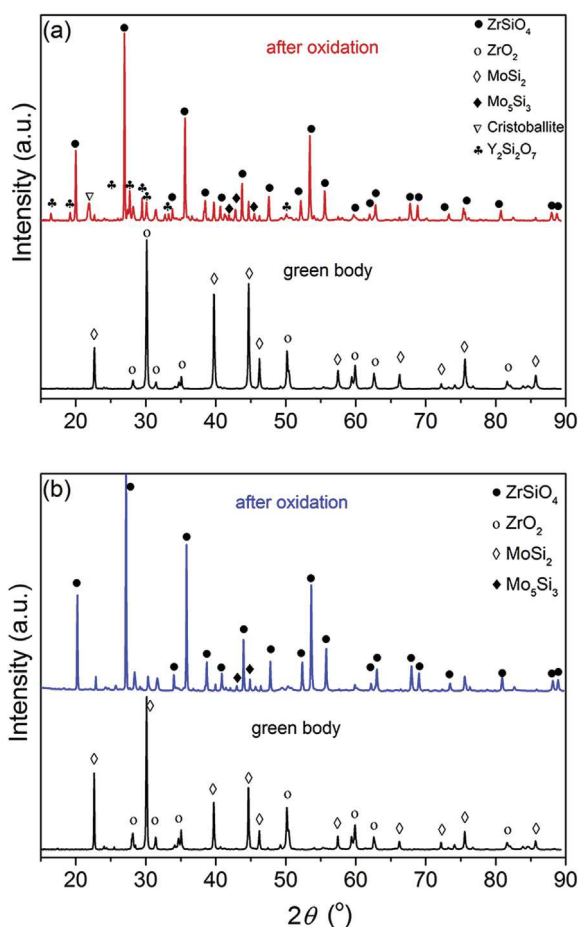


**Fig. 2.** X-ray diffraction patterns recorded with Cu-K $\alpha$  radiation of green tablets and after annealing at 1200 °C for 15 h in laboratory air: (a) YPSZ – MoSi<sub>2</sub> and (b) YPSZ – MoSi<sub>2</sub>(B) composite, respectively. (For interpretation of the references to colour in this figure legend, the reader is referred to the Web version of this article.)

force small [27], partitioning into m-ZrO<sub>2</sub> and c- ZrO<sub>2</sub> hardly occurs. This metastable phase is often referred to as tetragonal prime zirconia (t'-ZrO<sub>2</sub>).

The kinetics of the zircon formation strongly depends on the nature of the silica (i.e. amorphous or crystalline), which is related to the boron present in the MoSi<sub>2</sub> particles. The presence of boron atoms in the SiO<sub>2</sub> lattice decreases the viscosity of glassy silica by 3 orders magnitude [18,55]. Hence, the borosilicate spreads faster over the YPSZ surface than the boron-free amorphous silica. This ensures a better coverage of these particles by borosilicate than by silica [17,51], which results in a faster consumption of ZrO<sub>2</sub>; compare Fig. 3a with Fig. 3b.

Also, the kinetics of silica formation due to the oxidation of MoSi<sub>2</sub> is much faster when boron is present in the MoSi<sub>2</sub> particles; see Fig. 4. The intensity of the (200) diffraction line of ZrSiO<sub>4</sub> (having a body centered tetragonal crystal lattice) upon isothermal oxidation of the composite increases more rapidly when amorphous instead of crystalline silica was formed. For the YPSZ and MoSi<sub>2</sub> powder mixture, ZrO<sub>2</sub> is consumed rapidly at the beginning of the annealing process (i.e. the first hours); see Fig. 4a. A similar acceleration is observed for the YPSZ and boron containing MoSi<sub>2</sub> powder mixture, but the amount of ZrO<sub>2</sub> consumed and ZrSiO<sub>4</sub> formed is twice as high; see Fig. 4a and b. Once the empty space between the particles is filled with silica, the YPSZ particles are sealed off from the oxygen in the environment. In this case, oxygen can only reach the MoSi<sub>2</sub> particles via diffusion through the

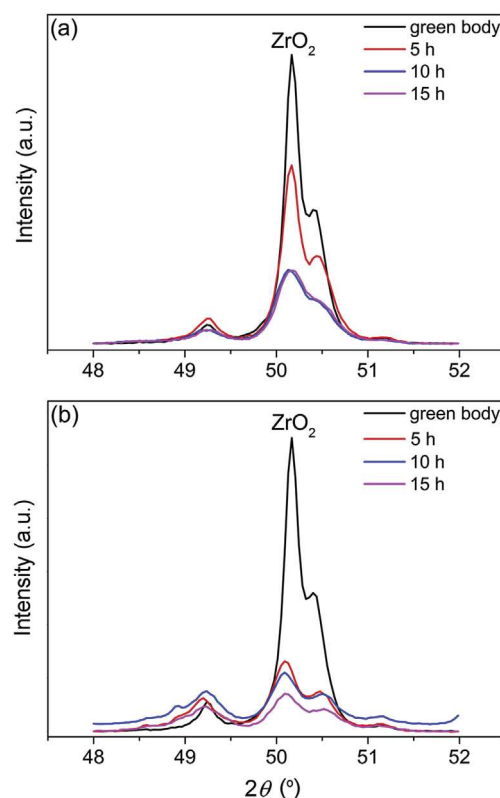


**Fig. 3.** X-ray diffraction lines recorded with Cu-K $\alpha$  radiation of the (112) and (020) monoclinic and tetragonal ZrO<sub>2</sub> peaks: (a) YPSZ – MoSi<sub>2</sub> and (b) YPSZ – MoSi<sub>2</sub>(B) composite after annealing at 1100 °C in laboratory air during 5, 10 and 15 h, respectively.

intergranular silica. Hence, the reaction decelerates after 2 h and ceases after 5 h of isothermal annealing at 1100 °C; see Fig. 4b.

### 3.2. Formation of silica or borosilicate and zircon in the bilayer system

Exposure of YPSZ – MoSi<sub>2</sub> bilayer system to high temperatures in air results in similar reaction products as observed in the compacted powder mixtures; cf. Section 3.1. A relatively thin layer of SiO<sub>2</sub> is formed in between the YPSZ and the MoSi<sub>2</sub>; see Fig. 5a. An irregular layer of ZrSiO<sub>4</sub> is formed in the YPSZ adjacent to the SiO<sub>2</sub> layer with some patches along YPSZ grain boundaries; see Fig. 5a. The observed bright zones in the remnant MoSi<sub>2</sub> layer correspond to the Mo<sub>5</sub>Si<sub>3</sub> phase (see Fig. 5a), which forms as a result of Si depletion from the original MoSi<sub>2</sub> due to oxidation. Upon very long exposure at 1100 °C in a high oxygen partial pressure environment further dissociation of Mo<sub>5</sub>Si<sub>3</sub> into (amorphous) SiO<sub>2</sub> will occur [3].

In the case of the YPSZ – MoSi<sub>2</sub>(B) bilayer system, an amorphous borosilicate layer is formed in between the YPSZ and the MoSi<sub>2</sub>(B); see Fig. 5b. Since the diffusion of oxygen through glassy borosilicate is faster than through B-free silica [56,61,62]; cf. Section 3.1, a thicker oxide layer is formed in comparison with the B-free system; see Fig. 4b. This amorphous silicate layer contains about 5 at.% B (see Fig. 6), suggesting that some of the B<sub>2</sub>O<sub>3</sub> reacts with SiO<sub>2</sub> to form borosilicate glass [56]. In addition, occasionally a yttrium borate phase, likely YBO<sub>3</sub> [59], is observed; see Fig. 6. Also, some B<sub>2</sub>O<sub>3</sub> reacts with Y<sub>2</sub>O<sub>3</sub> of the YPSZ; cf. Section 3.1. Finally, the amorphous borosilicate reacts with the ZrO<sub>2</sub> forming ZrSiO<sub>4</sub>; see Figs. 5b and 6. In this case, a more continuous and thicker zircon layer is formed in between the borosilicate and YPSZ as compared

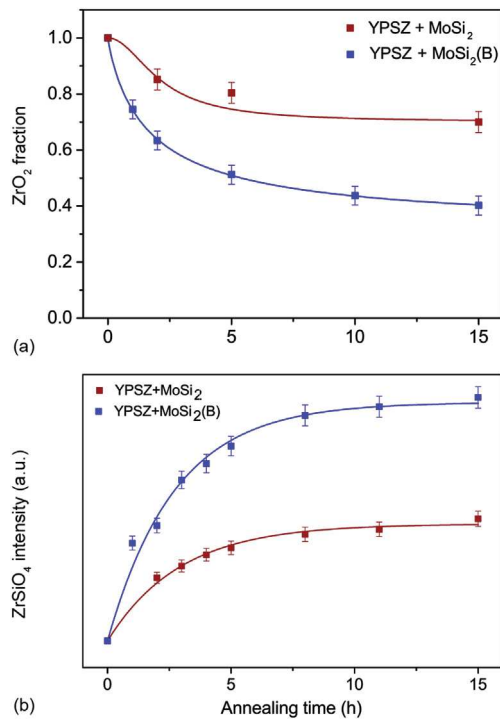


**Fig. 4.** Kinetic curves of (a) ZrO<sub>2</sub> consumption and (b) ZrSiO<sub>4</sub> formation in mixtures of YPSZ – MoSi<sub>2</sub> (red) and YPSZ – MoSi<sub>2</sub>(B) (blue) during annealing at 1100 °C in laboratory air as obtained from (ex situ) XRD analysis considering the (112) and (020) ZrO<sub>2</sub> and (200) ZrSiO<sub>4</sub> diffraction lines. Error corresponds to 3 times the standard deviation of the number of photons counted (Poissonian distribution). (For interpretation of the references to colour in this figure legend, the reader is referred to the Web version of this article.)

with the B-free system. Moreover, it can be seen that zircon forms along the grain boundaries of YPSZ, suggesting that silicon diffuses into YPSZ; see Fig. 7.

### 3.3. Kinetics of silica or borosilicate formation and zircon growth in bilayer system

At the high temperatures applied in this work, the growth rate of the silica and the zircon layers is expected to be controlled by diffusion of the reacting species through the developing SiO<sub>2</sub> or through the ZrSiO<sub>4</sub> layer. Then a parabolic growth rate law is applicable in both cases. The evolution of the thickness of borosilicate ( $x_1$ ) and zircon ( $x_2$ ) layer as a function of the oxidation time ( $t$ ) at 1100 °C in air are shown in Fig. 8. The initial thickness of silica and borosilicate layers after spark plasma sintering of the bilayer couples  $x_0$  is 1.0 and 2.9 μm, respectively. These closed layers may have prevented the formation of MoO<sub>3</sub>. It can be seen that B significantly enhances the kinetics of formation of both the silica and zircon layer.

The evolution of the borosilicate and zircon thicknesses at temperatures ranging from 1100 to 1300 °C, is shown in Fig. 9. As expected, the thickness of borosilicate and zircon layer is increasing with annealing temperature and exposure time.

## 4. Discussion

### 4.1. Mechanism of silica or borosilicate and zircon formation

It has been reported that the oxidation of MoSi<sub>2</sub> is controlled by the diffusion of oxygen ions or molecular di-oxygen through the

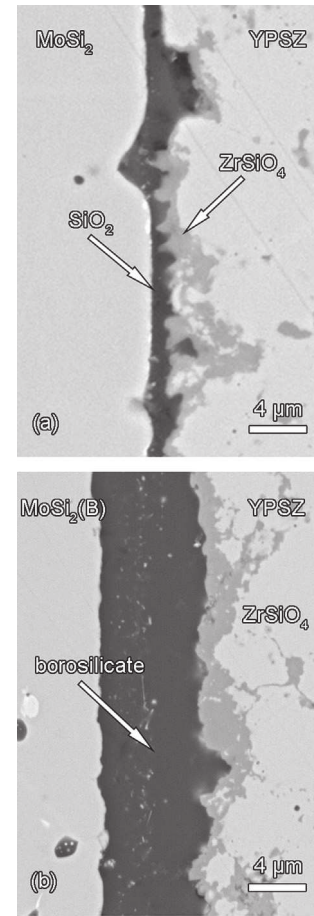


**Fig. 5.** SEM backscattered electron images of cross-section of (a) YPSZ – MoSi<sub>2</sub> and (b) YPSZ – MoSi<sub>2</sub>(B) interdiffusion couples after annealing for 96 h at 1100 °C in laboratory air. A silica layer (a) or borosilicate layer (b) is developed due to oxidation of MoSi<sub>2</sub> and MoSi<sub>2</sub>(B), respectively. The very small bright phase at the edge of MoSi<sub>2</sub> and MoSi<sub>2</sub>(B) belongs to Mo<sub>5</sub>Si<sub>3</sub>. In between the silica or borosilicate layer and the YPSZ, zircon (ZrSiO<sub>4</sub>) is formed.

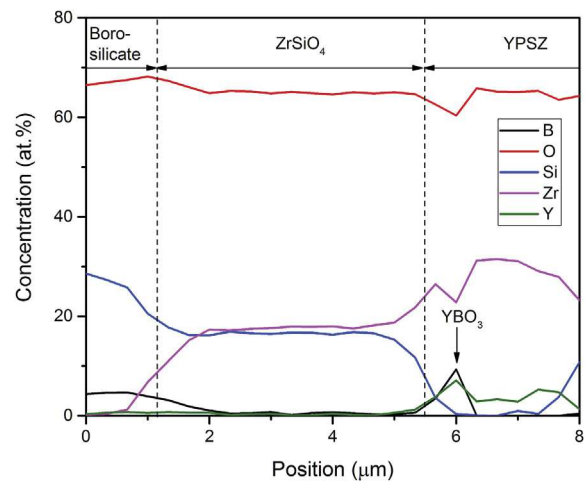


**Fig. 6.** Chemical composition profile across the YPSZ – MoSi<sub>2</sub>(B) interdiffusion couple after annealing at 1200 °C in laboratory air for 96 h, as obtained with EPMA. Error less than 0.5 at.% for each element.



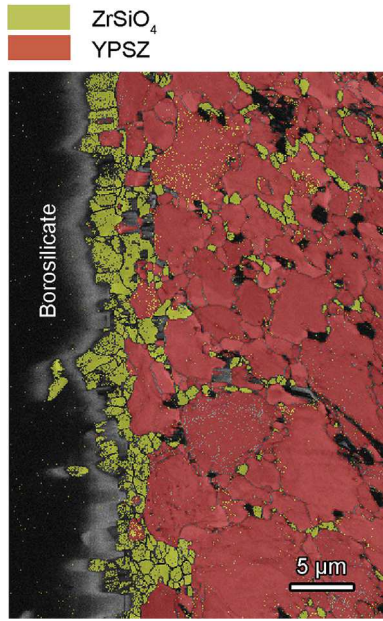


**Fig. 7.** Phase map of YPSZ-MoSi<sub>2</sub>(B) interdiffusion couple after annealing at 1200 °C in laboratory air for 96 h, showing the ZrSiO<sub>4</sub> formation at the YPSZ – SiO<sub>2</sub> + 5 at.% B interface and along grain boundaries of YPSZ as obtained by SEM –EBSD of a cross section.

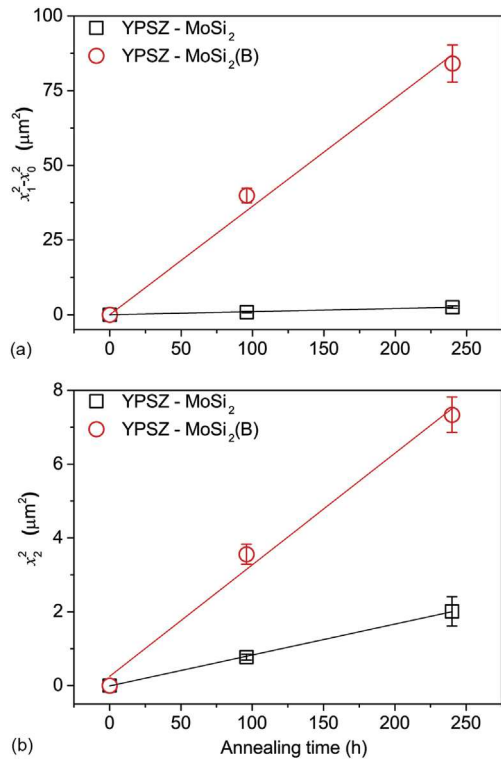


**Fig. 8.** Kinetics of (a) silica and borosilicate and (b) zircon layer growth in YPSZ- MoSi<sub>2</sub> and YPSZ – MoSi<sub>2</sub>(B) interdiffusion couples when annealing at 1100 °C in laboratory air. Error bars correspond to the standard deviation of the measured thickness. The initial thickness of silica and borosilicate layers after spark plasma sintering of the bilayer couples  $x_0$  is 1.0 and 2.9  $\mu\text{m}$ , respectively.

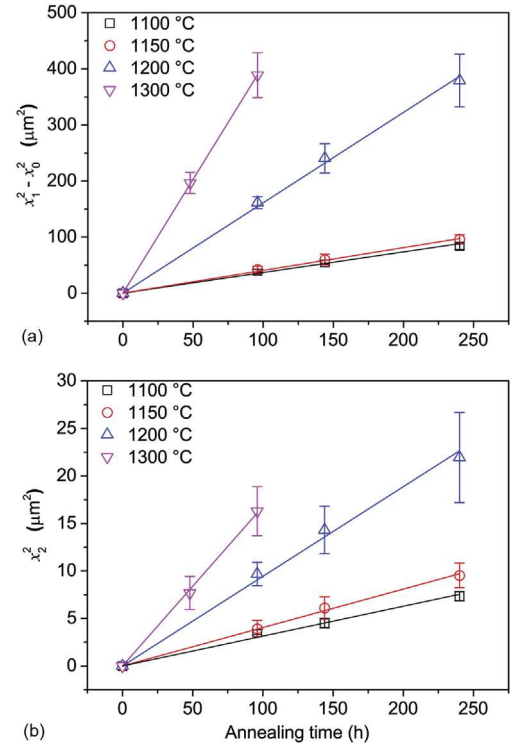


**Fig. 9.** The relation between the thickness of borosilicate ( $x_1$ ) and zircon ( $x_2$ ) layer and annealing time at different temperatures (from 1100 up to 1300 °C) of the YPSZ – MoSi<sub>2</sub>(B) bilayer system. Dashed lines correspond to the linear fitting of the experimental data for each temperature. Error bars correspond to the standard deviation of the measured thickness and  $x_0$  equals 2.9  $\mu\text{m}$ , which corresponds to the initial thickness of silica layer formed after the spark plasma sintering of the bilayer couple.

developing continuous silica layer [3,46,63]. The oxygen transport through crystalline and amorphous silica has been studied extensively [61,62,64]. The oxygen diffusion in amorphous SiO<sub>2</sub> is faster than in crystalline SiO<sub>2</sub>; see Fig. S3 in Supplementary Information. In addition, the presence of 5 at.% B in amorphous SiO<sub>2</sub> is reported to enhance the transport of oxygen through the borosilicate glass by 4 orders of magnitude than in boron free amorphous silica.

For continued formation of amorphous SiO<sub>2</sub>, oxygen has to diffuse through YPSZ and the developing ZrSiO<sub>4</sub> layer. The diffusion of oxygen in t-ZrO<sub>2</sub> is several orders of magnitude faster than in amorphous SiO<sub>2</sub> and hence is not rate limiting [62,65]; see Fig. S3 in Supplementary Information. But the diffusion of oxygen in ZrSiO<sub>4</sub> is of the same order of magnitude as in the amorphous SiO<sub>2</sub> [62,64,66]. Thus, for the bilayer system studied here, the oxygen diffusion either in the amorphous SiO<sub>2</sub> or in the ZrSiO<sub>4</sub> layer is the rate controlling factor for the silica formation.

Concerning the formation of zircon, either Si or Zr cations have to diffuse through the developing ZrSiO<sub>4</sub> layer. In the first case, zircon is formed at the ZrSiO<sub>4</sub> – YPSZ interface, while in the latter case, zircon is formed at the SiO<sub>2</sub> – ZrSiO<sub>4</sub> interface. According to studies by Cherniak [67] and Eppler [68], Si<sup>4+</sup> is the fastest diffusing cation in ZrSiO<sub>4</sub>. Hence, diffusion of Si<sup>4+</sup> through the zircon layer is thought to be the rate-limiting step of the zircon formation. This being the case, zircon would grow at the ZrSiO<sub>4</sub> – ZrO<sub>2</sub> interface. This is consistent with a few studies which attest that zircon precipitates at the ZrO<sub>2</sub> – ZrSiO<sub>4</sub> interface when the solubility limit of silicon in ZrO<sub>2</sub> is reached [4,6]. These studies assumed that zircon presents an over-stoichiometric silicon (ZrSi<sub>1+x</sub>O<sub>4-x</sub>) and vacancies at the oxygen sublattice (V<sub>O</sub><sup>••</sup>) [6], where interstitial silicon (Si<sub>i</sub><sup>••</sup>) are the fastest cationic species [6,66,68–70]. Since a parabolic kinetics



is observed for the growth of both the silica or borosilicate and zircon layer (see Figs. 8 and 9), the growth of these two layers is diffusion controlled rather than reaction kinetics controlled.

The  $\text{ZrSiO}_4$  forms at the  $\text{ZrO}_2$  -  $\text{ZrSiO}_4$  interface according to the following reaction:



For this reaction to proceed both  $\text{O}^{2-}$  and  $\text{Si}^{4+}$  ions must arrive at this interface. The oxygen ions originating from the gaseous environment can readily diffuse inward through the YPSZ layer [71]. The  $\text{Si}^{4+}$  ions coming from the silica or borosilicate layer diffuse through the  $\text{ZrSiO}_4$  layer, likely as an interstitial [67]. This implies dissociation of  $\text{SiO}_2$  at the  $\text{SiO}_2$ - $\text{ZrSiO}_4$  interface into  $\text{Si}^{4+}$  and  $\text{O}^{2-}$  ions. Since the oxygen potential at the  $\text{SiO}_2$ - $\text{ZrSiO}_4$  interface is higher than at the  $\text{MoSi}_2$ - $\text{SiO}_2$  interface, the oxygen ions diffuse through the silica layer towards the  $\text{MoSi}_2$ - $\text{SiO}_2$  interface and react with  $\text{MoSi}_2$  contributing to the growth of the silica or the borosilicate layer. Thus, the growth kinetics of the silica or the borosilicate layer also depends on the diffusion of the  $\text{Si}^{4+}$  ions through the zircon layer.

#### 4.2. Kinetic model for silica or borosilicate formation and zircon growth in bilayer system

The following model, schematically represented in Fig. 10, is proposed to explain the growth kinetics of the silica or borosilicate and zircon layer in the YPSZ -  $\text{MoSi}_2$  (with and without B) bilayer system. The advantage of this model is that it allows the assessment of the mechanisms that control the formation of the silica or the borosilicate and the growth of the zircon layer.

Two cases need to be considered. In the first case, diffusion of oxygen in the silica or borosilicate layer is the rate determining step for the silica and borosilicate formation, and the diffusion of silicon in the developing zircon layer is the rate determining step for the zircon formation. In the second case, diffusion of oxygen in zircon is controlling the growth of silica and the diffusion of silicon in zircon is controlling the growth rate of the zircon layer.

##### 4.2.1. Oxygen diffusion in silica or borosilicate being the rate-limiting step for silica growth

At temperatures above 1100 °C, oxidation of a bare  $\text{MoSi}_2$  substrate is known to be controlled by the slow diffusion of oxygen

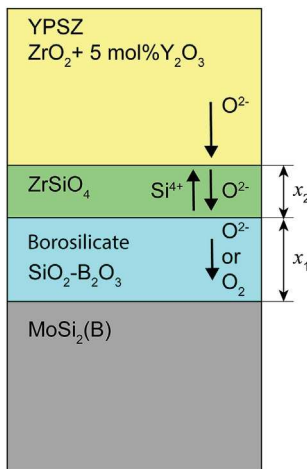


**Fig. 10.** Schematic of the transport phenomena associated with the formation of borosilicate and  $\text{ZrSiO}_4$  layers in the YPSZ -  $\text{MoSi}_2(\text{B})$  interdiffusion couples when exposed to high temperatures in air.

through the silica layer [46,72]. Then, for the growth or production ( $p$ ) of silica or borosilicate it can be written:

$$\left. \frac{dx_1}{dt} \right|_p = \frac{k_1}{2x_1} \quad (3)$$

where  $x_1$  is the thickness of the silica layer,  $t$  is the oxidation time and  $k_1$  the parabolic rate constant related to oxygen diffusion. Similarly, for the formation of zircon it can be written:

$$\left. \frac{dx_2}{dt} \right|_c = \frac{k_2}{2x_2} \quad (4)$$

where  $x_2$  is the thickness of the zircon layer and  $k_2$  the parabolic rate constant related to silicon diffusion in zircon. Since no zircon is present in the bilayer systems prior to annealing at high temperatures in air, i.e.  $x_2 = 0$  at  $t = 0$ , integration of Eq. (4) yields:

$$x_2 = \sqrt{k_2 \cdot t} \quad (5)$$

However, for the formation of zircon, part of the silica is consumed. The rate of this consumption ( $c$ ) is proportional to the zircon formation rate described by the parabolic rate constant  $k_2$ , cf. Eqs (4) and (5). The net ( $\Sigma$ ) thickening kinetics of the silica or borosilicate layer is obtained using Eqs (3) and (4), hence:

$$\left. \frac{dx_1}{dt} \right|_{\Sigma} = \left. \frac{dx_1}{dt} \right|_p - \left. \frac{dx_1}{dt} \right|_c = \frac{k_1}{2x_1} - \frac{k_2}{2x_2} \cdot \frac{V_{\text{SiO}_2}}{V_{\text{ZrSiO}_4}} \quad (6)$$

in which  $V_{\text{SiO}_2}$  and  $V_{\text{ZrSiO}_4}$  are the molar volumes of silica or borosilicate and zircon, respectively. For the molar volume of silica or borosilicate, the value of amorphous silica is taken and equals  $29 \text{ cm}^3 \text{ mol}^{-1}$  [2]. The molar volume of zircon is  $40 \text{ cm}^3 \text{ mol}^{-1}$  [73]. The physically consistent solution of Eq. (6) is given by:

$$x_1 = \sqrt{k_{\text{app}} \cdot t} \quad (7)$$

where  $k_{\text{app}}$  is the apparent parabolic rate constant. This parabolic rate constant is related to the overall mechanism involved in silica formation, i.e. production and consumption of silica. The rate constant  $k_1$  is directly related to the oxygen diffusion through the silica or borosilicate layer when it grows on the  $\text{MoSi}_2$  (B) itself. Combining Eqs (5)–(7), results in:

$$\left. \frac{dx_1}{dt} \right|_{\Sigma} = \frac{k_1}{2\sqrt{k_{\text{app}} \cdot t}} - \frac{\alpha \cdot \sqrt{k_2}}{2\sqrt{t}} = \frac{k_1}{\sqrt{k_{\text{app}}}} - \alpha \cdot \sqrt{k_2} \cdot \left( \frac{1}{2\sqrt{t}} \right) \quad (8)$$

where  $\alpha$  equals  $V_{\text{SiO}_2} / V_{\text{ZrSiO}_4}$ . This equation can be solved considering that in our experiments the thickness of the initial silica or borosilicate layer ( $x_0$ ) is small in comparison to the thickness upon prolonged oxidation ( $x_1$ ), i.e.  $x_0 \approx 0$  at  $t = 0$  (cf. Figs. 8a and 9a); hence:

$$x_1 = \left( \frac{k_1}{\sqrt{k_{\text{app}}}} - \alpha \cdot \sqrt{k_2} \right) \cdot \sqrt{t} \quad (9)$$

According to Eq. (9) the growth of silica in between  $\text{MoSi}_2$  (with and without B) and  $\text{ZrSiO}_4$  is described with a parabolic function, a prediction which agrees well with our experimental observations; see Figs. 8a and 9a. This implies that the proposed solution of Eq. (6), i.e. Eq. (7) is valid. When identifying the terms of Eqs (7) and (9), one obtains:

$$\sqrt{k_{app}} = \frac{k_1}{\sqrt{k_{app}}} - \alpha \cdot \sqrt{k_2} \quad (10)$$

Now, the apparent parabolic rate constant can be expressed explicitly in terms of  $k_1$  and  $k_2$ :

$$k_{app} = \frac{1}{2} \cdot \left[ \alpha^2 \cdot k_2 + 2k_1 - \alpha \cdot \sqrt{k_2(\alpha^2 \cdot k_2 + 4k_1)} \right] \quad (11)$$

The parabolic rate constant  $k_1$  can be calculated from the parabolic rate constants determined from the silica or borosilicate formation ( $k_{app}$ ) and the zircon formation ( $k_2$ ) in the bilayer systems; see Figs. 7–9, respectively. The relationship between these constants reads:

$$k_1 = k_{app} + \alpha \cdot \sqrt{k_2 \cdot k_{app}} \quad (12)$$

#### 4.2.2. Oxygen diffusion in zircon being the rate-limiting step for silica growth

If the diffusion of oxygen in the developing zircon layer is slower than in the silica or borosilicate layer, the growth of the latter will be determined by the rate of oxygen diffusion in zircon. Analogous to Eq. (6), for the net growth of the silica or borosilicate it can be written:

$$\left. \frac{dx_1}{dt} \right|_{\Sigma} = \frac{k_3}{2x_2} - \frac{k_2}{2x_2} \cdot \frac{V_{SiO_2}}{V_{ZrO_2}} \quad (13)$$

but now, with  $k_2$  and  $k_3$  as the parabolic rate constant pertaining to silicon diffusion and oxygen diffusion in zircon, respectively. A solution of Eq. (13) is obtained by considering that in our experiments the thickness of the initial silica or borosilicate layer ( $x_0$ ) is small compared with the thickness upon prolonged oxidation ( $x_1$ ), i.e.  $x_0 \approx 0$  at  $t = 0$  (cf. Eq. (9), hence:

$$x_1 = \frac{k_3 - \alpha \cdot \sqrt{k_2}}{\sqrt{k_2}} \cdot \sqrt{t} \quad (14)$$

Adopting Eq. (9), the apparent parabolic rate constant for the net growth of silica or borosilicate layer in the bilayer systems can be obtained:

$$\sqrt{k_{app}} = \frac{k_3}{\sqrt{k_{app}}} - \alpha \cdot \sqrt{k_2} \quad (15)$$

The relation between the parabolic rate constant  $k_3$  and the ones determined from the observed silica or borosilicate formation ( $k_{app}$ ) and zircon formation ( $k_2$ ) reads:

$$k_3 = \alpha \cdot k_2 + \sqrt{k_2 \cdot k_{app}} \quad (16)$$

#### 4.3. Analysis of observed silica or borosilicate and zircon growth kinetics in bilayer system

The observed kinetics of both silica or borosilicate and zircon formation in the YPSZ–MoSi<sub>2</sub> and the YPSZ–MoSi<sub>2</sub>(B) bilayer systems (presented in Figs. 8 and 9), is evaluated and quantified with the kinetic model presented in Section 4.2. The apparent parabolic growth rate constant,  $k_{app}$  (cf. Eq. (7)), can be obtained directly from the measured silica layer thicknesses versus annealing time of the YPSZ – MoSi<sub>2</sub> (with or without B) bilayer system; see Fig. 8a. The

presence of an initial silica layer (i.e.  $x_0$  the thickness at time  $t_0$ ) has to be taken into account, since a thin layer forms during the spark plasma sintering process of the bilayer system. Then, the  $k_{app}$  equation reads as:

$$x_1^2 - x_0^2 = k_{app} \cdot (t - t_0) \quad (17)$$

The parabolic rate constant  $k_2$ , cf. Eq. (5), is determined from the measured zircon layer thicknesses versus the annealing time; see Fig. 9b. The results for YPSZ – MoSi<sub>2</sub> without boron bilayer system annealed in air at 1100 °C are presented in Table 1. In addition, the parabolic rate constants pertaining to either oxygen diffusion in silica ( $k_1$ ) or oxygen diffusion in zircon ( $k_3$ ), which determines the growth of silica in the YPS–MoSi<sub>2</sub> boron free system (cf. Section 3.2) are evaluated using Eqs (12) and (16), respectively; see Table 1. The obtained results indicate that the ZrSiO<sub>4</sub> layer developed is too thin and not continuous (see Fig. 5a) and hence, its presence has a minor effect in controlling the further oxidation of the remaining MoSi<sub>2</sub>; see Table 1. Furthermore, the value of the parabolic constant  $k_1$  for the YPSZ–MoSi<sub>2</sub> bilayer system is in close agreement with the parabolic rate constant determined for the oxidation of MoSi<sub>2</sub> bulk in air at 1100 °C (i.e.  $1.1 \cdot 10^{-14} \text{ cm}^2 \text{ s}^{-1}$ ) [3,74]. Thus, our results suggest that for the system without boron the growth rate of silica is controlled by oxygen diffusion in silica.

For the YPSZ – MoSi<sub>2</sub>(B) bilayer system, the addition of 9 at.% of B leads to an increase of both the rate of borosilicate and that of zircon formation. The parabolic rate constants,  $k_{app}$  and  $k_2$ , increase by factor of 35 and 4, respectively, due to the presence of B in MoSi<sub>2</sub>. Clearly the diffusion of oxygen through borosilicate and zircon layer is enhanced by alloying MoSi<sub>2</sub> with boron; see Section 3.2. The former is due to the presence of B in the SiO<sub>2</sub> network, which alters the characteristics of silica glass [17]. Once B dissolves into silica, large [B<sub>5</sub>O<sub>6</sub>]<sup>3-</sup> ring segments develop inside the SiO<sub>2</sub> network and widen the [SiO<sub>4</sub>]<sup>4-</sup> tetrahedra [75], which accelerates the oxygen transport through the borosilicate layer. The latter is due to the more loose network in the borosilicate [17,51,61].

At 1100 °C, when boron is present in MoSi<sub>2</sub>,  $k_{app}$  and  $k_1$  increase by a factor of 35 and 23.5, respectively, while  $k_3$  value only increases by a factor of 8.6. This suggests that diffusion of oxygen through the amorphous SiO<sub>2</sub> layer controls the growth of the borosilicate scale.

In addition, the values of  $k_1$  are by factor of 1.2 larger than of  $k_{app}$ , for temperatures ranging from 1100 to 1300 °C, suggesting that the silica consumption to form zircon has only a small effect on the growth kinetics of silica. This holds irrespective of the presence of boron.

Since the diffusion of species at high temperatures in the bilayer systems is a thermally activated process, the temperature dependence of the parabolic rate constant can be described with an Arrhenius type equation:

$$k = A \exp(-E_A/RT) \quad (18)$$

where  $A$  is the pre-exponential factor, which is assumed to be temperature independent,  $R$  is the gas constant,  $T$  is the temperature and  $E_A$  is the activation energy. This holds for  $k_1$ ,  $k_2$  and  $k_3$ , which are related to the diffusion of single species. However,  $k_{app}$  may not follow the Arrhenius law (Eq. (18)) since it combines the effect of diffusion of two species. Nevertheless, as can be seen in Fig. 11 the  $k_{app}$  values do not differ much from the  $k_1$  values, an apparent activation energy can be evaluated from the  $k_{app}$  values.

The activation energies and pre-exponential factor were determined from the parabolic growth constants obtained for the YPSZ–MoSi<sub>2</sub>(B) bilayer system (see Fig. 11 and Table 1), and the results are summarized in Table 2. For the borosilicate formation dominated by oxygen diffusion in the silicate, an activation energy

**Table 1**

Parabolic rate constants  $k_{app}$ ,  $k_1$ ,  $k_2$  and  $k_3$  related to the growth of borosilicate and zircon layers in the YSZ – MoSi<sub>2</sub> and YSZ – MoSi<sub>2</sub>(B) interdiffusion systems.

Temperature (°C)			1100	1150	1200	1300
YPSZ/MoSi <sub>2</sub>	SiO <sub>2</sub>	$k_{app}$ (cm <sup>2</sup> s <sup>-1</sup> )	$2.9 \cdot 10^{-14}$	—	—	—
		$k_1$ (cm <sup>2</sup> s <sup>-1</sup> ) <sup>a</sup>	$5.1 \cdot 10^{-14}$	—	—	—
	ZrSiO <sub>4</sub>	$k_2$ (cm <sup>2</sup> s <sup>-1</sup> )	$2.3 \cdot 10^{-14}$	—	—	—
		$k_3$ (cm <sup>2</sup> s <sup>-1</sup> ) <sup>a</sup>	$4.2 \cdot 10^{-14}$	—	—	—
YPSZ/MoSi <sub>2</sub> -9 at.%B	SiO <sub>2</sub> with 5 at.%B	$k_{app}$ (cm <sup>2</sup> s <sup>-1</sup> )	$1.0 \cdot 10^{-12}$	$1.2 \cdot 10^{-12}$	$4.5 \cdot 10^{-12}$	$1.1 \cdot 10^{-11}$
		$k_1$ (cm <sup>2</sup> s <sup>-1</sup> ) <sup>a</sup>	$1.2 \cdot 10^{-12}$	$1.4 \cdot 10^{-12}$	$5.3 \cdot 10^{-12}$	$1.3 \cdot 10^{-11}$
	ZrSiO <sub>4</sub>	$k_2$ (cm <sup>2</sup> s <sup>-1</sup> )	$8.7 \cdot 10^{-14}$	$1.2 \cdot 10^{-13}$	$2.6 \cdot 10^{-13}$	$4.7 \cdot 10^{-13}$
		$k_3$ (cm <sup>2</sup> s <sup>-1</sup> ) <sup>a</sup>	$3.6 \cdot 10^{-13}$	$4.7 \cdot 10^{-13}$	$1.3 \cdot 10^{-12}$	$2.6 \cdot 10^{-12}$

<sup>a</sup> Calculated using Eqs. (12) and (16).

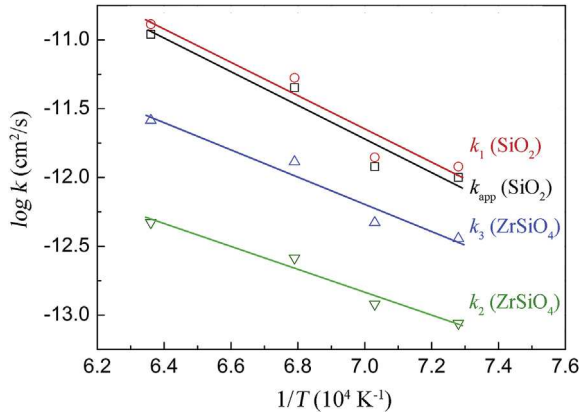


**Fig. 11.** Arrhenius plots of the rate constants  $k_1$ ,  $k_{app}$ ,  $k_2$  and  $k_3$  for the YSZ-MoSi<sub>2</sub>(B) interdiffusion couples. The activation energies and pre-exponential factors are obtained from linear fitting to the data points.

**Table 2**

Activation energy  $E_A$  and pre-exponential factor  $A$  of the thermally activated growth of the borosilicate and zircon layers in the YSZ – MoSi<sub>2</sub>(B) interdiffusion couple given by the parabolic rate constants  $k_{app}$ ,  $k_1$ ,  $k_2$  and  $k_3$ ; cf. Eq. (18).

Layer	$A$ (cm <sup>2</sup> /s)	$E_A$ (kJ/mol)
Net borosilicate growth ( $k_{app}$ )	$1.9 \cdot 10^{-8}$	$-228 \pm 42$
Borosilicate growth ( $k_1$ )	$1.9 \cdot 10^{-8}$	$-234 \pm 44$
Zircon growth by oxygen diffusion ( $k_2$ )	$9.8 \cdot 10^{-8}$	$-159 \pm 23$
Zircon growth by silicon diffusion ( $k_3$ )	$2.5 \cdot 10^{-6}$	$-190 \pm 31$

of  $234 \pm 44$  kJ mol<sup>-1</sup> and a pre-exponential factor of  $1.9 \cdot 10^{-8}$  cm<sup>2</sup> s<sup>-1</sup> are obtained. The value of the activation energy determined here is lower than those reported in the literature for the oxidation of bulk MoSi<sub>2</sub> (i.e.  $300 \div 340$  kJ mol<sup>-1</sup>) [46,76,77]. This is attributed to the structural characteristics of the borosilicate glass (i.e. the increased degree of [SiO<sub>4</sub>]<sup>4-</sup> deformation due to solubility of B in the SiO<sub>2</sub> network; also see Section 3.2 and Ref. [75]). As a result, the oxygen diffusion through the borosilicate layer is enhanced and therefore, a lower activation energy is attained for the YPSZ–MoSi<sub>2</sub>(B). The activation energy for the oxidation of isolated MoSi<sub>2</sub> particles containing 9 at.% B is even found to be about 2 times lower than the value obtained in this study (i.e. about 107 kJ mol<sup>-1</sup> determined for temperatures ranging between 1050 and 1200 °C).

An activation energy of  $159 \pm 23$  kJ mol<sup>-1</sup> and a pre-exponential factor of  $9.1 \cdot 10^{-8}$  cm<sup>2</sup> s<sup>-1</sup> are obtained for zircon formation. Since  $k_2$  is proportional to the silicon diffusion coefficient in zircon, the activation energy obtained from Eq. (18) can be compared with values reported in the literature and calculated from the self-diffusion coefficients of silicon in zircon. The activation energy for Si diffusion in zircon for MoSi<sub>2</sub> with 9 at.% B – YPSZ systems is

nearly 4.5 and 3.5 times lower than those obtained by Cherniak [67] and Zhang and Wu [66], while the activation energy calculated by Veytizou et al. [6] is 2 times higher than the one obtained in this study. The authors determined the rates of zircon formation via solid-state reaction of amorphous silica and tetragonal zirconia [6].

It is worth noting that both studies (i.e. Veytizou et al. [6] and Cherniak [67]) do not incorporate the effect of boron on the network of amorphous silica, nor on the kinetics of zircon formation. As documented, once B dissolves into silica network, it partially breaks the Si – O bond, leading to a weaker network than that of B free amorphous silica [17,51]. This likely makes the transport of Si<sup>4+</sup> interstitials easier and, hence explain the lower activation energy value for silicon diffusion in zircon for the YPSZ – MoSi<sub>2</sub>(B) bilayer system.

## 5. Conclusions

The formation mechanism and kinetics of both borosilicate and zircon in YPSZ – MoSi<sub>2</sub> (without B and with 9 at.% B) powder mixtures and bilayer systems were investigated. It is demonstrated that:

1. Zircon can be formed below 1200 °C in the YPSZ – MoSi<sub>2</sub> powder mixture or from the bilayer, irrespective of the prior presence of B in the MoSi<sub>2</sub>.
2. The presence of 9 at.% B in MoSi<sub>2</sub> prevents the crystallization of the amorphous SiO<sub>2</sub> formed and facilitates the formation of ZrSiO<sub>4</sub>, accelerating the reaction rate by factor of two (for the powder mixture) or four (for the bilayer).
3. The kinetics of the zircon formation as determined by annealing of the YPSZ/MoSi<sub>2</sub> bi-layered systems obeys a parabolic growth rate law. This is consistent with the diffusion of Si<sup>4+</sup> (likely Si<sup>4+</sup>) through the zircon layer being the growth rate depending step, rather than an (hypothetical) interfacial reaction (i.e. SiO<sub>2</sub> dissolution at SiO<sub>2</sub> – ZrSiO<sub>4</sub> interface or ZrSiO<sub>4</sub> formation at ZrSiO<sub>4</sub>/YPSZ interface).
4. The growth of the SiO<sub>2</sub> or SiO<sub>2</sub> – 5 at.% B oxide scales below ZrSiO<sub>4</sub> layer obeys a parabolic law. The kinetic model suggests that the diffusion of oxygen through the silica or borosilicate layer dominates the growth of the borosilicate scale.
5. The presence of B in MoSi<sub>2</sub> significantly increases the zircon and silica formation rates. At 1100 °C the parabolic rate constant for zircon formation increases by a factor of 4 when boron is present and the rate of silica formation by a factor of 35. The increase in both formation rates will accelerate the crack healing in YPSZ with embedded B-containing MoSi<sub>2</sub> particles.

The kinetic data as obtained in this work are crucial for quantitative modelling of the healing kinetics and the lifetime extension for extrinsic self-healing YPSZ thermal barrier coatings containing healing particles of the compositions studied here.

## Acknowledgments

This project has received funding from European Union Seventh Framework Program (FP7/2007–2013) under grant agreement no. 309849, SAMBA. The authors thank Ing. R. W. A. Hendrikx for the XRD analysis.

## Appendix A. Supplementary data

Supplementary data to this article can be found online at <https://doi.org/10.1016/j.actamat.2019.05.046>.

## References

- [1] W.G. Sloof, S.R. Turteltaub, A.L. Carabat, Z. Derelioglu, P. S.A. G.M. Song, Crack healing in yttria stabilized zirconia thermal barrier coatings, in: S. van der Zwaag, E. Brinkman (Eds.), *Self Healing Materials: Pioneering Research in the Netherlands*, IOS Press, Amsterdam, 2015, pp. 217–225.
- [2] Z. Derelioglu, A.L. Carabat, G.M. Song, S. van der Zwaag, W.G. Sloof, On the use of B-alloyed MoSi<sub>2</sub> particles as crack healing agents in yttria stabilized zirconia thermal barrier coatings, *J. Eur. Ceram. Soc.* 35 (16) (2015) 4507–4511.
- [3] S. Knittel, S. Mathieu, M. Vilasi, The oxidation behaviour of uniaxial hot pressed MoSi<sub>2</sub> in air from 400 to 1400 degrees C, *Intermetallics* 19 (8) (2011) 1207–1215.
- [4] T. Itoh, formation of polycrystalline zircon (ZrSiO<sub>4</sub>) from amorphous silica and amorphous zirconia, *J. Cryst. Growth* 125 (1–2) (1992) 223–228.
- [5] T. Mori, H. Yamamura, H. Kobayashi, T. Mitamura, formation mechanism of ZrSiO<sub>4</sub> powders, *J. Mater. Sci.* 28 (18) (1993) 4970–4973.
- [6] C. Veytizou, J.F. Quinson, O. Valfort, G. Thomas, Zircon formation from amorphous silica and tetragonal zirconia: kinetic study and modelling, *Solid State Ionics* 139 (3–4) (2001) 315–323.
- [7] M. Meyer, M. Kramer, M. Akinc, Boron-doped molybdenum silicides, *Adv. Mater.* 8 (1) (1996) 85–88.
- [8] M.K. Meyer, M. Akinc, Isothermal oxidation behavior of Mo-Si-B intermetallics at 1450°C, *J. Am. Ceram. Soc.* 79 (10) (1996) 2763–2766.
- [9] M.K. Meyer, M. Akinc, Oxidation behavior of boron-modified Mo<sub>5</sub>Si<sub>3</sub> at 800–1300°C, *J. Am. Ceram. Soc.* 79 (4) (1996) 938–944.
- [10] M. Akinc, M.K. Meyer, M.J. Kramer, A.J. Thom, J.J. Huebsch, B. Cook, Boron-doped molybdenum silicides for structural applications, *Mater. Sci. Eng. A* 261 (1–2) (1999) 16–23.
- [11] Z. Tang, A.J. Thom, M.J. Kramer, M. Akinc, Characterization and oxidation behavior of silicide coating on multiphase Mo-Si-B alloy, *Intermetallics* 16 (9) (2008) 1125–1133.
- [12] P.R. Taleghani, S. Bakhshi, M. Erfanmanesh, G. Borhani, R. Vafaei, Improvement of MoSi<sub>2</sub> Oxidation Resistance via Boron Addition: Fabrication of MoB/MoSi<sub>2</sub> Composite by Mechanical Alloying and Subsequent Reactive Sintering, 2014.
- [13] P. Mandal, A.J. Thom, M.J. Kramer, V. Behrani, M. Akinc, Oxidation behavior of Mo-Si-B alloys in wet air, *Mater. Sci. Eng. A* 371 (1–2) (2004) 335–342.
- [14] C.G. McKamey, P.F. Tortorelli, J.H. DeVan, C.A. Carmichael, A study of pest oxidation in polycrystalline MoSi<sub>2</sub>, *J. Mater. Res.* 7 (10) (1992) 2747–2755.
- [15] T.C. Chou, T.G. Nieh, Mechanism of MoSi<sub>2</sub> pest during low temperature oxidation, *J. Mater. Res.* 8 (1) (1993) 214–226.
- [16] A.J. Thom, E. Summers, M. Akinc, Oxidation behavior of extruded Mo<sub>5</sub>Si<sub>3</sub>B<sub>x</sub>-MoSi<sub>2</sub>-MoB intermetallics from 600–1600 °C, *Intermetallics* 10 (6) (2002) 555–570.
- [17] F. Monteverde, A. Bellosi, Oxidation of ZrB<sub>2</sub>-based ceramics in dry air, *J. Electrochem. Soc.* 150 (11) (2003) B552–B559.
- [18] T. Karahan, G. Ouyang, P.K. Ray, M.J. Kramer, M. Akinc, Oxidation mechanism of W substituted Mo-Si-B alloys, *Intermetallics* 87 (2017) 38–44.
- [19] K. Kochubey, W.G. Sloof, Self Healing Mechanism in Thermal Barrier Coatings, ITSC 2008, DVS-Verlag GmbH, Maastricht, The Netherlands, 2008.
- [20] D. Koch, G. Mauer, R. Vaßen, Manufacturing of composite coatings by atmospheric plasma spraying using different feed-stock materials as YSZ and MoSi<sub>2</sub>, *J. Therm. Spray Technol.* 26 (4) (2017) 708–716.
- [21] F. Nozahic, C. Estournès, A.L. Carabat, W.G. Sloof, S. van der Zwaag, D. Monceau, Self-healing thermal barrier coating systems fabricated by spark plasma sintering, *Mater. Des.* 143 (2018) 204–213.
- [22] Y. Chen, X. Zhang, S. van der Zwaag, W.G. Sloof, P. Xiao, Damage evolution in a self-healing air plasma sprayed thermal barrier coating containing self-shielding MoSi<sub>2</sub> particles, *J. Am. Ceram. Soc.* (2019), <https://doi.org/10.1111/jace.16313> in press.
- [23] N.P. Padture, M. Gell, E.H. Jordan, Thermal barrier coatings for gas-turbine engine applications, *Science* 296 (5566) (2002) 280–284.
- [24] D.R. Clarke, S.R. Phillpot, Thermal barrier coating materials, *Mater. Today* 8 (6) (2005) 22–29.
- [25] M. Belmonte, Advanced ceramic materials for high temperature applications, *Adv. Eng. Mater.* 8 (8) (2006) 693–703.
- [26] F. Cernuschi, P. Bison, A. Moscatelli, Microstructural characterization of porous thermal barrier coatings by laser flash technique, *Acta Mater.* 57 (12) (2009) 3460–3471.
- [27] D.R. Clarke, C.G. Levi, Materials design for the next generation thermal barrier coatings, *Annu. Rev. Mater. Res.* 33 (1) (2003) 383–417.
- [28] R.T. Wu, K. Kawagishi, H. Harada, R.C. Reed, The retention of thermal barrier coating systems on single-crystal superalloys: effects of substrate composition, *Acta Mater.* 56 (14) (2008) 3622–3629.
- [29] X. Zhang, J. Kulczyk-Malecka, J. Carr, P. Xiao, P.J. Withers, 3D characterization of porosity in an air plasma-sprayed thermal barrier coating and its effect on thermal conductivity, *J. Am. Ceram. Soc.* 101 (6) (2018) 2482–2492.
- [30] J.T. DeMasi-Marcin, D.K. Gupta, Protective coatings in the gas turbine engine, *Surf. Coating. Technol.* 68 (1994) 1–9.
- [31] M.A. Alvin, K. Klotz, B. McMordie, D. Zhu, B. Gleeson, B. Warnes, Extreme temperature coatings for future gas turbine engines, *J. Eng. Gas Turbines Power* 136 (11) (2014).
- [32] E.P. Busso, J. Lin, S. Sakurai, A mechanistic study of oxidation-induced degradation in a plasma-sprayed thermal barrier coating system.: Part II: life prediction model, *Acta Mater.* 49 (9) (2001) 1529–1536.
- [33] C. Li, X. Zhang, Y. Chen, J. Carr, S. Jacques, J. Behnken, M. di Michiel, P. Xiao, R. Cernik, Understanding the residual stress distribution through the thickness of atmosphere plasma sprayed (APS) thermal barrier coatings (TBCs) by high energy synchrotron XRD; digital image correlation (DIC) and image based modelling, *Acta Mater.* 132 (2017) 1–12.
- [34] M. Mutter, G. Mauer, R. Mücke, O. Guillon, R. Vaßen, Systematic investigation on the influence of spray parameters on the mechanical properties of atmospheric plasma-sprayed YSZ coatings, *J. Therm. Spray Technol.* 27 (4) (2018) 566–580.
- [35] J. Kulczyk-Malecka, X. Zhang, J. Carr, F. Nozahic, C. Estournès, D. Monceau, A.L. Carabat, W.G. Sloof, S. van der Zwaag, P.J. Withers, P. Xiao, Thermo – mechanical properties of SPS produced self-healing thermal barrier coatings containing pure and alloyed MoSi<sub>2</sub> particles, *J. Eur. Ceram. Soc.* 38 (12) (2018) 4268–4275.
- [36] A. Rabiei, A.G. Evans, Failure mechanisms associated with the thermally grown oxide in plasma-sprayed thermal barrier coatings, *Acta Mater.* 48 (15) (2000) 3963–3976.
- [37] A.G. Evans, D.R. Mumm, J.W. Hutchinson, G.H. Meier, F.S. Pettit, Mechanisms controlling the durability of thermal barrier coatings, *Prog. Mater. Sci.* 46 (5) (2001) 505–553.
- [38] K.W. Schlichting, N.P. Padture, E.H. Jordan, M. Gell, Failure modes in plasma-sprayed thermal barrier coatings, *Materials Science and Engineering A-Structural Materials Properties Microstructure and Processing* 342 (1–2) (2003) 120–130.
- [39] X. Chen, J.W. Hutchinson, M.Y. He, A.G. Evans, On the propagation and coalescence of delamination cracks in compressed coatings: with application to thermal barrier systems, *Acta Mater.* 51 (7) (2003) 2017–2030.
- [40] L.B. Chen, Yttria-stabilized zirconia thermal barrier coatings - a review, *Surf. Rev. Lett.* 13 (5) (2006) 535–544.
- [41] H. Echsler, V. Shemet, M. Schütze, L. Singheiser, W.J. Quadackers, Cracking in and around the thermally grown oxide in thermal barrier coatings: a comparison of isothermal and cyclic oxidation, *J. Mater. Sci.* 41 (4) (2006) 1047–1058.
- [42] D. Liu, M. Seraffon, P.E.J. Flewitt, N.J. Simms, J.R. Nicholls, D.S. Rickerby, Effect of substrate curvature on residual stresses and failure modes of an air plasma sprayed thermal barrier coating system, *J. Eur. Ceram. Soc.* 33 (15–16) (2013) 3345–3357.
- [43] M.D. Hager, P. Greil, C. Leyens, S. van der Zwaag, U.S. Schubert, Self-healing materials, *Adv. Mater.* 22 (47) (2010) 5424–5430.
- [44] F. Nozahic, D. Monceau, C. Estournès, Thermal cycling and reactivity of a MoSi<sub>2</sub>/ZrO<sub>2</sub> composite designed for self-healing thermal barrier coatings, *Mater. Des.* 94 (2016) 444–448.
- [45] J.T. Armstrong, Quantitative elemental analysis of individual microparticles with electron beam instruments, in: K.F.J. Heinrich, D.E. Newbury (Eds.), *Electron Probe Quantitation*, Springer US, Boston, MA, 1991, pp. 261–315.
- [46] C.D. Wirkus, D.R. Wilder, High-temperature oxidation of molybdenum disilicide, *J. Am. Ceram. Soc.* 49 (4) (1966) 173–&.
- [47] Y.T. Zhu, M. Stan, S.D. Conzone, D.P. Butt, Thermal oxidation kinetics of MoSi<sub>2</sub>-based powders, *J. Am. Ceram. Soc.* 82 (10) (1999) 2785–2790.
- [48] Y.T. Zhu, L. Shu, D.P. Butt, Kinetics and products of molybdenum disilicide powder oxidation, *J. Am. Ceram. Soc.* 85 (2) (2002) 507–509.
- [49] S. Lohfeld, M. Schütze, Oxidation behaviour of particle reinforced MoSi<sub>2</sub> composites at temperatures up to 1700°C. Part I: literature review, *Mater. Corros.* 56 (2) (2005) 93–97.
- [50] E.F. Riebling, Structure of borosilicate and borogermanate melts at 1300°C: a viscosity and density study, *J. Am. Ceram. Soc.* 47 (10) (1964) 478–483.
- [51] F. Monteverde, A. Bellosi, The resistance to oxidation of an HfB<sub>2</sub>-SiC composite, *J. Eur. Ceram. Soc.* 25 (7) (2005) 1025–1031.
- [52] R. Sakidja, J.S. Park, J. Hamann, J.H. Perepezko, Synthesis of oxidation resistant silicide coatings on Mo-Si-B alloys, *Scripta Mater.* 53 (6) (2005) 723–728.
- [53] R. Sakidja, J.H. Perepezko, S. Kim, N. Sekido, Phase stability and structural defects in high-temperature Mo-Si-B alloys, *Acta Mater.* 56 (18) (2008) 5223–5244.
- [54] F.A. Rioult, S.D. Imhoff, R. Sakidja, J.H. Perepezko, Transient oxidation of Mo-Si-B alloys: effect of the microstructure size scale, *Acta Mater.* 57 (15) (2009) 4600–4613.
- [55] J.A. Lemberg, R.O. Ritchie, Mo-Si-B alloys for ultrahigh-temperature structural applications, *Adv. Mater.* 24 (26) (2012) 3445–3480.



- [56] D. Li, Z. Yang, D. Jia, X. Duan, S. Wang, Q. Zhu, Y. Miao, J. Rao, Y. Zhou, Effects of boron addition on the high temperature oxidation resistance of dense sSiBCN monoliths at 1500°C, *Corros. Sci.* 126 (2017) 10–25.
- [57] D.M. Cupid, H.J. Seifert, Thermodynamic calculations and phase stabilities in the Y-Si-C-O system, *J. Phase Equilibria Diffusion* 28 (1) (2007) 90–100.
- [58] G. Ouyang, P.K. Ray, S. Thimmaiah, M.J. Kramer, M. Akinc, P. Ritt, J.H. Perepezko, Oxidation resistance of a Mo-W-Si-B alloy at 1000–1300°C: the effect of a multicomponent Mo-Si-B coating, *Appl. Surf. Sci.* 470 (2019) 289–295.
- [59] D.Z. de Florio, R. Muccillo, Effect of boron oxide on the cubic-to-monoclinic phase transition in yttria-stabilized zirconia, *Mater. Res. Bull.* 39 (10) (2004) 1539–1548.
- [60] H.G. Scott, Phase relationships in the zirconia-yttria system, *J. Mater. Sci.* 10 (1975) 1527–1535.
- [61] J. Schlichting, Glasses and Glass Ceramics from Gels Oxygen transport through glass layers formed by a gel process, *J. Non-Cryst. Solids* 63 (1) (1984) 173–181.
- [62] M.A. Lamkin, F.L. Riley, R.J. Fordham, Oxygen mobility in silicon dioxide and silicate glasses: a review, *J. Eur. Ceram. Soc.* 10 (5) (1992) 347–367.
- [63] Y.Q. Liu, G. Shao, P. Tsakirooulos, On the oxidation behaviour of MoSi<sub>2</sub>, *Intermetallics* 9 (2) (2001) 125–136.
- [64] E.B. Watson, D.J. Cherniak, Oxygen diffusion in zircon, *Earth Planet. Sci. Lett.* 148 (3–4) (1997) 527–544.
- [65] M.S. Khan, M.S. Islam, D.R. Bates, Cation doping and oxygen diffusion in zirconia: a combined atomistic simulation and molecular dynamics study, *J. Mater. Chem.* 8 (10) (1998) 2299–2307.
- [66] B.H. Zhang, X.P. Wu, Prediction of self-diffusion and heterodiffusion coefficients in zircon, *J. Asian Earth Sci.* 42 (1–2) (2011) 134–141.
- [67] D.J. Cherniak, Si diffusion in zircon, *Phys. Chem. Miner.* 35 (4) (2008) 179–187.
- [68] R.A. Eppler, Mechanism of formation of zircon stains, *J. Am. Ceram. Soc.* 53 (8) (1970) 457–&.
- [69] K.M. Trappen, R.A. Eppler, Reaction of zirconia with silica at the stoichiometry of zircon, *J. Am. Ceram. Soc.* 72 (6) (1989) 882–885.
- [70] A. Kaiser, M. Lobert, R. Telle, Thermal stability of zircon (ZrSiO<sub>4</sub>), *J. Eur. Ceram. Soc.* 28 (11) (2008) 2199–2211.
- [71] M. Kilo, C. Argirusis, G. Borchardt, R.A. Jackson, Oxygen diffusion in yttria stabilised zirconia - experimental results and molecular dynamics calculations, *Phys. Chem. Chem. Phys.* 5 (11) (2003) 2219–2224.
- [72] J.S. Park, R. Sakidja, J.H. Perepezko, Coating designs for oxidation control of Mo-Si-B alloys, *Scripta Mater.* 46 (11) (2002) 765–770.
- [73] P.C. P. K. Villars, Pearson's crystal data: crystal structure database for inorganic compounds, *ASM International* 9 (2008).
- [74] S. Melsheimer, M. Fietzek, V. Kolarik, A. Rahmel, M. Schutze, Oxidation of the intermetallics MoSi<sub>2</sub> and TiSi<sub>2</sub> - a comparison, *Oxid. Metals* 47 (1–2) (1997) 139–203.
- [75] J. Schlichting, Oxygen transport through silica surface layers on silicon-containing ceramic materials, *High. Temp. - High. Press.* 14 (6) (1982) 717–724.
- [76] E.W. Sucov, Diffusion of oxygen in vitreous silica, *J. Am. Ceram. Soc.* 46 (1) (1963) 14–20.
- [77] A.A. Sharif, High-temperature oxidation of MoSi<sub>2</sub>, *J. Mater. Sci.* 45 (4) (2010) 865–870.